Microporous and Mesoporous Materials

Faster transport in hollow zeolites

--Manuscript Draft--

Manuscript Number:	MICMAT-D-20-01065R1
Article Type:	Full length article
Keywords:	Zeolites Diffusion through porous media Zero Length Column
Corresponding Author:	David FARRUSSENG, PhD CNRS Villeurbanne, FRANCE
First Author:	Ana Rita Morgado Prates, PhD
Order of Authors:	Ana Rita Morgado Prates, PhD
	Cecile Daniel, Doctor
	Céline Pagis
	Yves Schuurman
	Alain Tuel
	David FARRUSSENG, PhD
Abstract:	Nano-zeolites and hierarchical zeolites have shown enhanced transport properties that are generally attributed to a shorter diffusion path length (L). However, the concomitant increase in the external surface of these types of zeolites may also affect overall transport as the interfaces may act as diffusion barriers. Recently, hollow zeolite crystals have been presented as an alternative zeolite morphology. They possess a large inner cavity and an overall size and shape similar to those of plain microporous zeolite. In contrast to classic hierarchical zeolite materials, the inner cavity of the hollow zeolite induces a shortened diffusion path length with no effect on external surface area. In this work, we have studied the impact of diffusion path length on transport properties by comparing the characteristic time of transport of hydrocarbons in plain zeolite crystals and their hollow counterparts, using zero-length column (ZLC) measurements. Our results show that hollow morphology doubles or quadruples the transport speed for Silicalite-1 and Beta zeolites, respectively. Compared to other reports focusing on nanosized or hierarchical zeolites, this study is free of any bias due to major modifications in external surface area, because hollow and plain zeolites have very similar crystal dimensions.

Powered by Editorial Manager® and ProduXion Manager® from Aries Systems Corporation

Cover Letter

Dr. David Farrusseng
IRCELYON
Tel : +33 6 32 37 86 17
david.farrusseng@ircelyon.univ-lyon1.fr

Dear Mr. Schmidt

Nano-zeolites and hierarchical zeolites have shown enhanced transport properties that are generally attributed to a shorter diffusion path length (L). However, the concomitant increase in the external surface may lead to the creation of diffusion surface barriers, which may provide erroneous conclusions to the transport properties.

In here, we study molecular diffusion of hydrocarbons in zeolites with different diffusion path lengths (L), while keeping the same crystal size, i.e. same external surface. This is possible using hollow zeolites and its homologous plain zeolites: the inner cavity of the hollow zeolite reduces the thickness of the crystal (L), while keeping the same external surface. Toluene was chosen as probe molecule for hollow and plain Silicalite-1 samples, while cyclohexane was used for hollow and plain Beta samples. Transport properties are studied by comparing the characteristic diffusion time of the hydrocarbon in hollow and plain samples, which is obtained using the Zero-Length Column technique.

We demonstrate in this article that hollow zeolites allow faster transport than plain zeolites due to the shortening of diffusion path length and importantly for same particle dimensions ie. with the same external surface area. For hollow Silicalite-1, the transport is doubled, while for hollow Beta zeolite it is quadrupled for crystals of very similar sizes and without a secondary porous network – attesting to the relevancy of this study.

We believe that the originality of this study will be a valuable participation in Microporous and Mesoporous Materials journal. Thank you for your consideration.

Sincerely

David Farrusseng

Dear Prof Kleitz,

Please find below our list of revision.

However, as you can see below, the reviewer 1 is commenting the paper beyond the scope of the study rather than addressing clear questions .

We have open this discussion in our last section parts where this particular topic was already addressed .

Best regards

Dr. D. Farrusseng

Reviewer #1: Referee Report MICMAT-D-20-01065 on „Faster Transport …" by Morgado et al.
Hollow zeolites represent an intriguing novel class of microporous materials with numerous options for technological application with improved transport properties. The present paper provides a thorough comparison of "plain" and hollow zeolites with respect to their transport properties, notably, by comparing the desorption rates as resulting by the application of the ZLC technique. The paper is thus, doubtlessly, dealing with a timely topic of practical relevance. It is well written, with the Journal of Microporous and Mesoporous Materials offering the relevant audience, and I warmly recommend publication. There are, however, a couple of points that I wanted to point out to the authors for being taken account of on their revising the MS.

Molecular uptake and release on microporous materials is today known to be often influenced and, sometimes, even controlled by the finite permeability through the crystal surface, i.e. by "surface barriers", as a property inherent nanoporous materials quite in general, of different (material-specific) intensity. Thanks to the advent of the techniques of microimaging, we dispose of the option to determine - with well-shaped crystals - even quite accurately their magnitude. Though, most likely, the sizes of the crystals investigated in this study (additionally aggravated by the dispersion in their appearance) will not allow such estimates,

RESPONSE

We do not agree here. The size of the crystals is very homogeneous as it can be shown on the pictures and also shown in our prior papers

it is quintessential to refer to this option and to mention that mass transfer may, as well, be affected by surface barriers.

RESPONSE

Surface barriers are mentioned twice in the introduction and specifically addressed in the discussion part.

Page 1 :" As the **external surface area** of such zeolites is correspondingly increased, however, **diffusion barriers** may increase as well, thereby hindering overall transport [14-16]. This is illustrated by several examples in the literature in which **the impact of surface barriers** is often associated with small crystal sizes that are characterized by a high external surface area"

Page 12 ". The authors assumed that **external surface barriers are the dominant mechanism** in diffusion, which prevails on intracrystalline diffusion in smaller crystals "

For quantifying the simultaneous influence of diffusion and surface permeation on the overall release (and uptake) time, the method of moments (introduced in Barrer's classical textbook about "Zeolites and Clay Minerals as Sorbents and Molecular Sieves", Academic Press, London, 1978., see also section 13.6.2 in J. Kärger, D.M. Ruthven, and D.N. Theodorou, "Diffusion in Nanoporous Materials", Wiley - VCH, Weinheim, 2012) has proved to serve as a most helpful formalism. For spheres it yields, in the limiting cases of diffusion and barrier control for the respective time constants, $\tau_{diff}=R^2/15D$ and $\tau_{barr}=R/3\alpha$ and, under the simultaneous influence of both resistances, simply their sum $\tau_{overall}=\tau_{diff}+\tau_{barr}$, with R (= L in the present paper) meaning the effective particle radius and α the surface permeability (also referred to as surface permeance). The so far, probably, most accurate data correlating the resistances of surface permeation and bulk diffusion in zeolite MFI have been provided by L. Gueudré et al. with "Micro-Imaging by Interference Microscopy: A Case Study of Orientation-Dependent Guest Diffusion in MFI-Type Zeolite Host Crystals" in Materials (open access) 5 (2012) 721-740. With crystals exceeding the sizes of the present ones by more than one order of magnitude, τ_{barr} (as a measure of the barrier resistance) was found to be of the order of τ_{diff} for benzene and methyl-butane (and to even exceed the τ_{diff} by one order of magnitude for 4-methyl-2-pentyne). With decreasing sizes, as a consequence of their different size dependencies, the influence of surface resistances in relation to intracrystallinde diffusion is further increasing. Thus, in the present studies, the influence of surface barriers must be expected to be of at least the same order of magnitude as the diffusional resistances.

RESPONSE

This discussion is out of scope.

By referring, with the notation Deff, to an effective diffusivity rather than to the genuine intracrystalline diffusivity D, the authors allow for the inclusion of further transport resistances, including surface barriers. With the nomenclature $\tau=L^2/D_{eff}$ as used by the authors, and with the above relations for τ_{diff} and τ_{barr}, the effective diffusivity, as introduced in the present paper, would thus be found to obey the relation $D_{eff}^{-1}=D^{-1}+5/(\alpha L)$. In the limiting case of barrier limitation, in place of the present Eq.1, one would, correspondingly, obtain proportionality between the time constants and the diffusion path lengths $\tau_H/\tau_p=L_H/L_p$. The values of L_H/L_p that one would attain in this way were between 0.5 and 0.66 for silicalite and between 0.17 and 0.36 for beta and, hence, also in the range of microscopic data.

RESPONSE

We agree that this point. Instead of developing the approach, we prefer to go directly to the conclusion of this remark. We have added the following sentence at the end of our discussion
"We want also to stress that surface barrier contribution cannot be ruled out in the case of cyclohexane. In the case it would occur, it would be a minor contribution to the overall resistance which cannot be quantified here taking into account of size dispersion of the crystals."

Since for one and the same zeolite material, the surface permeability (permeance) is known to, possibly, vary even more significantly than the intracrystalline diffusivity (see, e.g., J.C.S. Remi et al. "The role of crystal diversity in understanding mass transfer in nanoporous materials", Nat. Mater. 15 (2015) 401-406, as a matter of course, also this type of estimate can be only considered as an order-of-magnitude estimate. But also this estimate would nicely confirm the conclusions of the authors, namely, that also in the (more likely) case of barrier limitation, (effective) diffusivity data and the message of microscopic imaging on transport enhancement do reasonable well agree.

RESPONSE

It is unclear what shall be addressed here.

There are a few, quite formal, issues which the authors should also look at:
In Eq. B4, in the last term, time t is missing;

RESPONSE: Checked!

The nomenclature "B1 …" in section C (rather than "C1 …"), used for designating the equations, occurred, most likely, in error

RESPONSE: modified accordingly

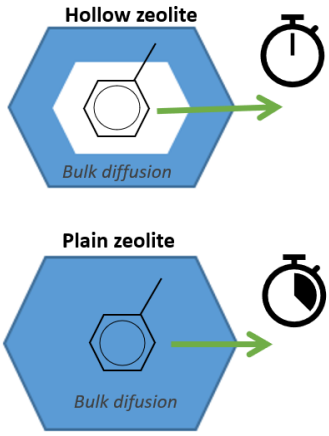
The origin of indicating intervals (rather than a single value) for L_H/L_p in Tab. 4, in addition to the indicated error, is not obvious since Tabs 2 and 3 provide only one value for τ_H and τ_L from which the values for L_H/L_p are determined. Their uncertainty would be expected to appear in the error, which is anyway indicated.

RESPONSE: unclear! But no problems in the end!

Highlights

- Hollow zeolites allow faster transport than plain zeolites
- The faster transport is directly linked to the shortening of diffusion path length.
- While keeping hollow and plain zeolite crystals with the same crystal size, we can investigate the impact of a different diffusion path length, without bias from different external surface area.

Graphical Abstract



3 Main results

- Hollow zeolites allow faster transport than plain zeolites
- The faster transport is directly linked to the shortening of diffusion path length..
- While keeping hollow and plain zeolite crystals with the same crystal size, we can investigate the impact of a different diffusion path length, without bias from different external surface area.

Manuscript-revised

Click here to view linked References

Click here to access/download;Manuscript;Faster transport in hollow zeolites_revised.docx

Faster transport in hollow zeolites

Ana Rita Morgado Prates[a], Cécile Daniel[a], Céline Pagis[a,b], Yves Schuurman[a], Alain Tuel[a], David Farrusseng[a]

a) Univ Lyon, Université Claude Bernard Lyon 1, CNRS, IRCELYON, F-69626, Villeurbanne, France

b) IFP Energies Nouvelles, Etablissement de Lyon, BP3, 69360, Solaize, France

ABSTRACT

Nano-zeolites and hierarchical zeolites have shown enhanced transport properties that are generally attributed to a shorter diffusion path length (L). However, the concomitant increase in the external surface of these types of zeolites may also affect overall transport as the interfaces may act as diffusion barriers. Recently, hollow zeolite crystals have been presented as an alternative zeolite morphology. They possess a large inner cavity and an overall size and shape similar to those of plain microporous zeolite. In contrast to classic hierarchical zeolite materials, the inner cavity of the hollow zeolite induces a shortened diffusion path length with no effect on external surface area. In this work, we have studied the impact of diffusion path length on transport properties by comparing the characteristic time of transport of hydrocarbons in plain zeolite crystals and their hollow counterparts, using zero-length column (ZLC) measurements. Our results show that hollow morphology doubles or quadruples the transport speed for Silicalite-1 and Beta zeolites, respectively. Compared to other reports focusing on nanosized or hierarchical zeolites, this study is free of any bias due to major modifications in external surface area, because hollow and plain zeolites have very similar crystal dimensions.

1. Introduction

Catalytic conversion in microporous catalysts such as zeolites can be severely limited by diffusion, especially in the case of bulky substrates[1]. Consequently, the design of multimodal porous zeolite materials has become a major solution combining the catalytic features of the microporous zeolite with enhanced diffusion through a secondary pore network[1–3]. In the literature, two different approaches to the design of such “mesoporous” zeolites have been investigated: i) the creation of hierarchical porous structures with intra-particle mesopores by demetallation[4,5] and ii) the synthesis of nanocrystals (< 100 nm) with extra-particle voids[6–9] (Fig. 1). Both approaches yield materials made of smaller microporous zeolite domains and therefore with shorter diffusion path lengths (L) that mitigate transport limitations of catalytic conversion[10].

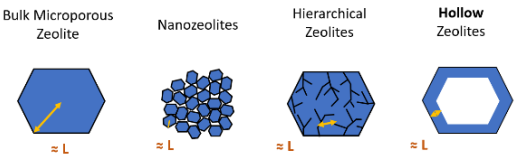


Figure 1: Diagram of different crystal morphologies.

In the literature, nano-zeolites and hierarchical zeolites have shown enhanced transport properties compared to their conventional counterpart that could be correlated with a shorter diffusion path length, (L) [10–13]. As the external surface area of such zeolites is correspondingly increased, however, diffusion barriers may increase as well, thereby hindering overall transport [14–

16]. This is illustrated by several examples in the literature in which the impact of surface barriers is often associated with small crystal sizes that are characterized by a high external surface area. Gueudré *et al*.[16] carried out gravimetric uptake measurements by cyclohexane adsorption on Silicalite-1 with different crystal sizes from 0.4 µm up to 17 µm of mean radius. For large crystals the effective diffusion coefficients (D_{eff}) were equal, as can be expected for crystals with the same porous structure. For crystals smaller than 2 µm, however, D_{eff} were found to be much smaller (by about one order of magnitude). Also, in the case of small crystals, major variations were found from one type to another. In the case of 2-µm Silicalite-1 crystals, surface resistance represented 60% of the total mass transfer resistance, leading to a smaller D_{eff} value than that of larger crystals. Teixeira *et al*.[14] studied the sorption kinetics of cyclohexane in Silicalite-1 (MFI) samples of sizes covering a wide range from 80 nm to 3 µm. Similarly to Gueudré *et al*.[16], the authors observed a reduction in D_{eff} as the crystal size decreased, which they attributed to an increase in surface barriers. Duncan *et al*.[15] measured the sorption kinetics of cyclohexane in different ZSM-5 samples using the zero-length column method. Very similar values of D_{eff} and of effective diffusion energy (E_d) were found for all crystal sizes, which ranged from 4 to 24 µm. In all cases, their D_{eff} values were superior to those of Teixeira *et al.* Also, Li *et al*.[11] obtained very different D_{eff} values for ZSM-5 crystals of 800 nm or 100 nm and for multilamellar structures composed of 2-nm-thick sheets. From these studies carried out on relatively large model crystals, we can conclude that the effective diffusion coefficient depends on the crystal size, especially for small crystals (< 2 µm), possibly due to surface barrier phenomena that vary along with the external surface area of the crystals. For hierarchical zeolites or nanozeolites whose external surface area can attain as much as 50% of the microporous surface area[17], we can assume that the size effect on effective diffusion could be even greater. More importantly, we can question whether the enhanced catalytic activities observed for hierarchical zeolites or nanozeolites are due to shorter path lengths (L) or to faster effective diffusion (D_{eff}) as expressed in the Thiele modulus principle.

Recently, hollow zeolite crystals have been presented as an alternative zeolite morphology[18,19], see Figure 1. Crystals of this type possess a large inner cavity and an overall size and shape similar to those of plain microporous zeolite. In contrast to classic hierarchical zeolite materials, L is shortened due to the presence of the inner cavity, while the external surface area remains unchanged. In the literature, hollow Y zeolite has already shown improved catalytic activity and effectiveness compared to equivalent plain Y zeolite in cracking and hydroisomerization reactions, thanks to its shorter L[20,21].

In this work, we have examined the impact of diffusion path length on transport properties by comparing the characteristic time of transport of hydrocarbons in plain zeolite crystals and their hollow counterparts. We show that for Silicalite-1 and Beta zeolites respectively, the hollow morphology doubles or quadruples the characteristic transport speed. Compared to other studies of nanosized hierarchical zeolites, this study is not biased by major modifications in external surface area, as hollow and plain zeolites have crystals of very similar sizes**.** To this end, we made a special effort to synthesize plain and hollow zeolites with similar sizes and compositions. The characteristic diffusion time (τ) of zeolite samples was measured by the zero-length column technique. Assuming that the diffusion constant was the same for hollow and plain zeolites, we estimated diffusion path lengths via the ZLC technique ($\mathbf{L_D}$) and compared them with the equivalent radius of crystals observed by microscopy images ($\mathbf{R_{eq}}$).

2. Experimental Section

2.1. Synthesis of Zeolites

Hollow Silicalite-1 crystals were synthesized as in our previous publications[22,23] and further denoted as **HollowS-1**. The synthesis procedure mainly consists in the dissolution-recrystallization of bulk Silicalite-1 crystals, further denoted **PlainS-1**, using tetrapropylammonium hydroxide solutions as desilicating medium. Under such conditions, very regular hollow structures are obtained with a wall thickness of ca. 30-50 nm and external dimensions close to those of the original **PlainS-1** crystals.

The **HollowBeta** sample was synthesized according to our previous work[18], using a seed-assisted organic structure directing agent (OSDA)-free synthesis with CIT-6 crystals as seeds. The calcined crystals were exchanged twice with a 2M NaCl solution (NaCl>99.5%, Fluka), 0.1 gzeol /ml, in order to ensure the greatest elimination of protons. The ion exchange process was carried out at 70 °C for 2h, under vigorous stirring. The dispersion was centrifuged and the solid washed and dried overnight at 80 °C.

Contrary to the Silicalite-1 samples, we could not use the parent CIT-6 crystal as the corresponding plain Beta due to different framework compositions (CIT-6 is a zincosilicate, while **HollowBeta** is an aluminosilicate). Faced with the difficulty of synthesizing a single plain zeolite sharing the same characteristics of **HollowBeta** with respect to Si/Al ratio, crystal size and external morphology, two reference ***BEA** zeolites were synthesized, **PlainBeta1** and **PlainBeta2**, each of them matching most of the above criteria.

PlainBeta1 was first prepared following a recipe reported by Zheng *et al.*[24]. A gel of Beta zeolite was first prepared with molar composition of the gel: 2.2 Na_2O : 20SiO_2 : Al_2O_3 : 4.6 $(TEA)_2O$: 2.3 $(NH_4)_2O$: 401 H_2O. Initially, 0.64 g of NaOH, 18.07 g of TEABr (Sigma Aldrich> 98 wt. %) and 1.76 g of $NaAlO_2$ (Honeywell Riedel-de Haën, Al_2O_3 : 50–56 (53 wt. %) Na_2O : 40–45 (42 wt. %) were dissolved in 36.7 g of distilled water, followed by the addition of 5.63 ml of NH_4OH Sigma Aldrich, 25 wt. %NH_3 in H_2O). Ludox HS-30 Sigma Aldrich (36.70 g) was added slowly with vigorous stirring. The mixture was stirred at room temperature for 2 h, then transferred into a 100 mL autoclave and kept at 140 °C for 10 days without stirring. The obtained zeolite was filtered, washed with distilled water and dried at 80°C. The as-made crystals were exchanged with a 2M NaCl solution, 0.1 g_{zeol}/ml, similarly to **HollowBeta** sample. Then, calcination was carried out in air at 550 °C for 4h hours with a heating rate of 87.5 °C/h followed by another ion-exchange with NaCl in similar conditions.

PlainBeta2 synthesis was based on the method reported by Ding *et al.*[25] A gel of Beta zeolite was first prepared with molar composition of the gel: 10.5 TEAOH : 50 SiO_2 : Al_2O_3 : 750 H_2O. Initially, 9.6 ml of TEAOH 35% were mixed with 23.6 ml of distilled water. After stirring, the solution is split into solution A and solution B (10 ml of solution). Then, 6.67 g of Aerosil 200 (Evonik Industries > 98,9 wt. %) was slowly added to solution A with vigorous stirring. Then, Al powder (Sigma Aldrich> 99 wt. %) (0.12 g) were dissolved in solution B, with vigorous stirring for 10 min. Finally, solution A and B are mixed and stirred at room temperature for 4 h. Then the gel was transferred into two 48 mL autoclave and kept at 140 °C for 7 days while stirring. The obtained zeolite was centrifuged, washed with distilled water and dried at 80 °C. Calcination step and ion-exchange step were carried out similarly to **HollowBeta** sample.

It is important to note that Beta samples were ion-exchanged with NaCl to prevent chemical reactions during diffusion tests.

2.2. Characterization techniques

Samples were characterized using standard techniques. X-ray powder diffraction (XRD) patterns were recorded at room temperature on a D8 advance A25 diffractometer (Cu Kα1 radiation) from 4 to 80° with 0.02° steps and 0.5 s per step. Chemical compositions were obtained by ICPOES after solubilization of the solids in HF-HCl solutions. Scanning Electron Microscope (SEM) images were collected on an FEI ESEM-XL30 microscope under high vacuum (FEG source). A high voltage of 20 kV was used in order to enhance the contrast between regions of the crystals with different densities, which revealed the existence of hollow structures. TEM images were obtained on a JEOL 2010 LaB6 microscope operating at 200 kV. The average dimensions of the crystals were obtained using IMAGEJ software from the observation of at least 200 crystals for each sample. Nitrogen adsorption-desorption isotherms were measured at 77 K on a Belsorp-mini (BEL-Japan) sorption device. Approximately 80 mg of sample were outgassed under vacuum in a cell at 300°C overnight prior to adsorption. The microporous volume was determined as the volume of N_2 adsorbed for very low partial pressures, more precisely when the slope of adsorption branch became lower than 10^3 $cm^3(STP)g^{-1}$.

2.3. Zero-Length Column Method

The **zero-length column** method was chosen to measure diffusion in this study. This technique determines the effective diffusion coefficient (D_{eff}) of a given sorbate in a zeolite packed-bed cell, analyzing the respective transient desorption curve. It is a common technique for measuring the diffusion of hydrocarbons over zeolite materials since it is sensitive to the typical characteristic diffusion times. Using a sufficiently high fluid velocity, the external resistances of heat and mass transfers can be negligible. ZLC has the particularity of using a very thin packed bed of zeolite ("zero-length"), which eliminates the contribution of axial dispersion resistance. As a result, ZLC is known as an appropriate technique for measuring intracrystalline diffusion, which includes all types of transfer resistance within the zeolite crystals. The ZLC setup and measurement protocol used in this work (see Appendix D) is similar to the one developed by Eic and Ruthven in their previous works[26]. A small amount of sample (1-2 mg) was placed in the ZLC cell, which consisted of a 1/8" Swagelok union. The zeolite sample was sandwiched between two porous stainless steel sintered disks with the same diameter, placed inside the Swagelok union. The ZLC cell was placed in a gas chromatograph oven (Agilent, 6850 Series GC system) whose effluent stream was continuously monitored by a flame ionization detector (FID). We chose to characterize the transport of cyclohexane over hollow and plain Beta zeolite samples, and the transport of toluene over hollow and plain Silicalite-1 zeolites. The ZLC measurements for toluene and cyclohexane were carried out at 40, 50 and 60°C and at 80, 100 and 120°C respectively. Before each set of runs, the sample was activated overnight under high helium flow at 300°C. The adsorption step was conducted under low relative partial pressures at 0.192 kPa and 0.05 kPa for cyclohexane and toluene, respectively, until equilibrium was reached. The experimental curves were fitted to the ZLC model, considering a spherical shape, for high purge flow and long desorption times, which corresponds to equation B4 (see Appendix C). The characteristic time (τ) was measured from the fitting of the ZLC model. A high flow was applied in order to establish diffusion-controlled regime conditions[14]. The L_{ZLC} value was used as an indicator that the runs were carried out in the kinetic regime (see Appendix E).

Mean diffusion path lengths were estimated by the ZLC technique and denoted by the symbol $\mathbf{L_D}$, while corrected dimensions of the particles were estimated by microcopy image analysis and hereafter denoted $\mathbf{R_{eq}}$. For plain zeolites, $\mathbf{R_{eq}}$ is the equivalent radius of a sphere at isovolume of the crystalline particle, whereas for hollow zeolites, $\mathbf{R_{eq}}$ is estimated from the wall thickness. For

the sake of simplicity, the subscript H or P will be used to refer to hollow and plain zeolites, respectively. The mean path diffusion path length will be noted $\mathbf{L_H}$ and $\mathbf{L_P}$, while the equivalent radius will be noted $\mathbf{R_H}$ and $\mathbf{R_P}$. For plain zeolites, the effective diffusion constants ($\mathbf{D_{eff}}$) were estimated from the formula $\boldsymbol{\tau = R_P^2/D_{eff}}$.

3. Results

Table *1* summarizes the main chemical and structural characteristics of the plain and hollow zeolites. Additional data such as TEM and SEM images, XRD patterns and N_2 isotherms are presented in Appendix B. Plain and hollow samples are highly crystalline for the **MFI** type structure, with no extra crystalline phases[22,23]. Similarly, to **PlainS-1, HollowS-1** is pure Si zeolite, as no Al sources were added during the synthesis. TEM images of the synthesized **PlainS-1** and **HollowS-1 zeolites** show that both samples are homogeneous in size, with crystals featuring hexagonal prisms with a smooth surface. **HollowS-1** crystals are slightly larger than **PlainS-1** as a result of the re-crystallization of dissolved species on the outer surface, as already described in previous works[22]. The dimensions of the crystals on average are 75 nm for the hexagonal side length (a) and 98 nm for the height (H) for **PlainS-1,** and 93 and 120 nm for **HollowS-1** (Table *1*). TEM images revealed that 20-30% of the hollow crystals presented several inner cavities, denoted hereafter as ***multi-hollow crystals***. Whether these cavities are isolated from each other or communicate via small mesopores in zeolite walls is unknown. N_2 adsorption isotherms present a type I adsorption branch with similar V_{micro} of 0.13 cm^3/g for **PlainS-1** and 0.12 cm^3/g for **HollowS 1** (see Appendix A). The large hysteresis loop of **HollowS-1** has been attributed to the presence of an internal cavity that communicates with the surface via zeolite micropores[22]. For **PlainS-1**, the equivalent radius $\boldsymbol{R_P}$ **= 70 nm** has been estimated from the radius of a sphere with an equivalent volume of $1{,}43 \times 10^6$ nm^3 measured by the physical dimensions (a and H). For the **HollowS-1**, $\mathbf{R_H}$ is the wall thickness, averaging 40 nm.

XRD data show that the Beta samples synthesized herein are pure and highly crystalline with patterns characteristic of ***BEA** type structures (see Appendix B). **HollowBeta** and **PlainBeta1** have approximately the same Si/Al ratio (~10), while **PlainBeta2** has a lower Al content (Si/Al = 22) (see Table *1*). The Na/Al ratio lies between 0.4 and 0.7, indicating that around half of the negative charges of framework Al atoms are compensated by protons. N_2 adsorption isotherms (see Figure B *4*) show that the three samples present a type I adsorption branch as expected. The three Beta zeolites possess similar V_{micro} values, of 0.17±0.02 cm^3/g, which is in very good agreement with literature data[18,24,25,27,28] (seeTable *1*). **PlainBeta1** of average external dimension of 1.2 µm exhibits a rough surface (see Appendix B). In contrast, **PlainBeta2** and **HollowBeta** present the same truncated octahedral morphology, pine tree-shaped on each side, but different average crystal sizes of 0.7 and 1.2 µm respectively. Considering the **PlainBeta1** as an ellipsoid with average radii values of 0.44 and 0.61 µm (see Figure B *3*), the radius of the corresponding sphere is calculated to be $\mathbf{R_P}$ **= 490 nm.** For **PlainBeta2** with truncated octahedral morphology, the equivalent radius is estimated to be $\mathbf{R_P}$ **= 330 nm**. The inner cavity of **HollowBeta** is clearly observed in TEM images, from the contrast between the center and the external part of the crystals, as already reported for hollow Beta in our previous work[18]. The average wall thickness $\mathbf{R_H}$ is estimated to be equal to **150 nm** from TEM images. It should be noted that a small proportion (~10%) of the hollow crystals were found to be broken because of the severe mixing during ion exchange with NaCl (see Figure B *2*).

Table 1 - Physical characteristics of Silicalite-1 samples and Beta samples.

Sample name	PlainS-1	HollowS-1	PlainBeta1	PlainBeta2	HollowBeta
Si/Al (-)	Pure Si	Pure Si	10.9	22.1	8.7
Na/Al	-	-	0.5	0.4	0.7
V_{micro} (cm^3/g)	0.13	0.12	0.15	0.18	0.16
Average Crystal Size (nm)	a - 75 H - 98	a - 93 H - 120	1210	650	1150
External Crystal Shape					
R_{eq} **(nm)**	70	40	490	330	150

A first glance at the time scale shows that hollow zeolites desorb much faster than their plain counterparts (Figure *2*). For Silicalite-1 zeolites, the concentration c/c_0 of 0.01 is achieved in 400 s for **HollowS-1** versus 730 s for **PlainS-1.** The difference is even more pronounced for Beta zeolites. The concentration c/c_0 of 0.001 is achieved in 250 s for **HollowBeta**, compared to 1600 s for **PlainBeta1** and 1300 s for **PlainBeta2.** Despite structural differences of the two plain Beta reference zeolites in terms of Si/Al ratio and external shape, we can observe very similar desorption curves. We can therefore assume that the observed differences in ZLC desorption curves between hollow and plain samples arise mainly from the difference in diffusion path length of the samples, which is directly linked to the dimension feature of the crystals between plain and hollow morphologies.

The ZLC responses and model fits as a function of temperature are shown in the linear region in Figure *3* and Figure *4*. For both systems, the fitting lines have an excellent agreement with the experimental data. As expected, the characteristic diffusion times (τ) estimated from the ZLC model for hollow zeolites are much shorter than those of the corresponding plain zeolites (see Table *2* andTable *3*). For Silicalite-1 samples at 40°C, the diffusion time τ is half as long for the hollow zeolite as for the plain zeolite. The reduction is even more pronounced for **HollowBeta2,** with an average decrease of one fifth at 80°C with respect to plain Beta zeolites. Faster transport in hollow zeolites is observed regardless of the measurement temperatures. Over the temperature range studied, we can observe for **HollowS-1** and **HollowBeta** a decrease of 34-49% and 64-78%, respectively.

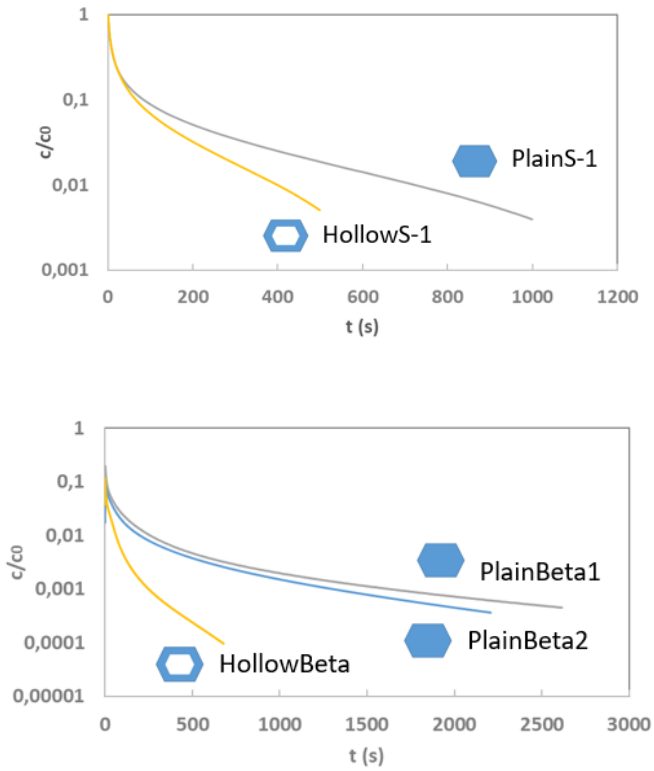


Figure 2 – Experimental ZLC data for toluene in Silicalite-1 samples at 40ºC, and experimental ZLC data for cyclohexane in Beta samples at 80ºC

.

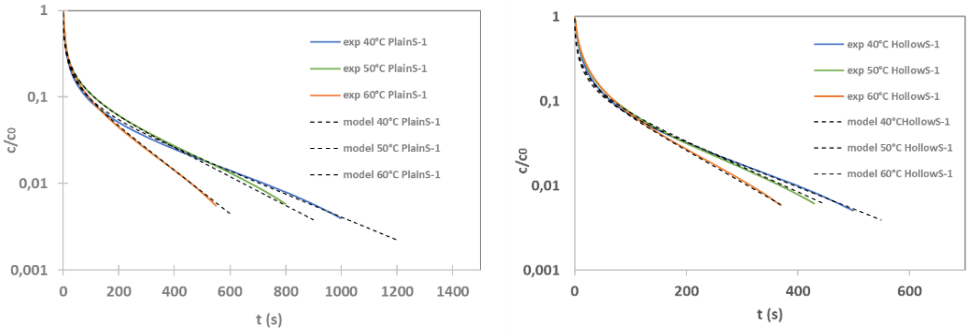


Figure 3 - Experimental ZLC data (plain lines) and theoretical ZLC curves (dashed lines) for toluene in Silicalite-1 samples at 40, 50 & 60°C.

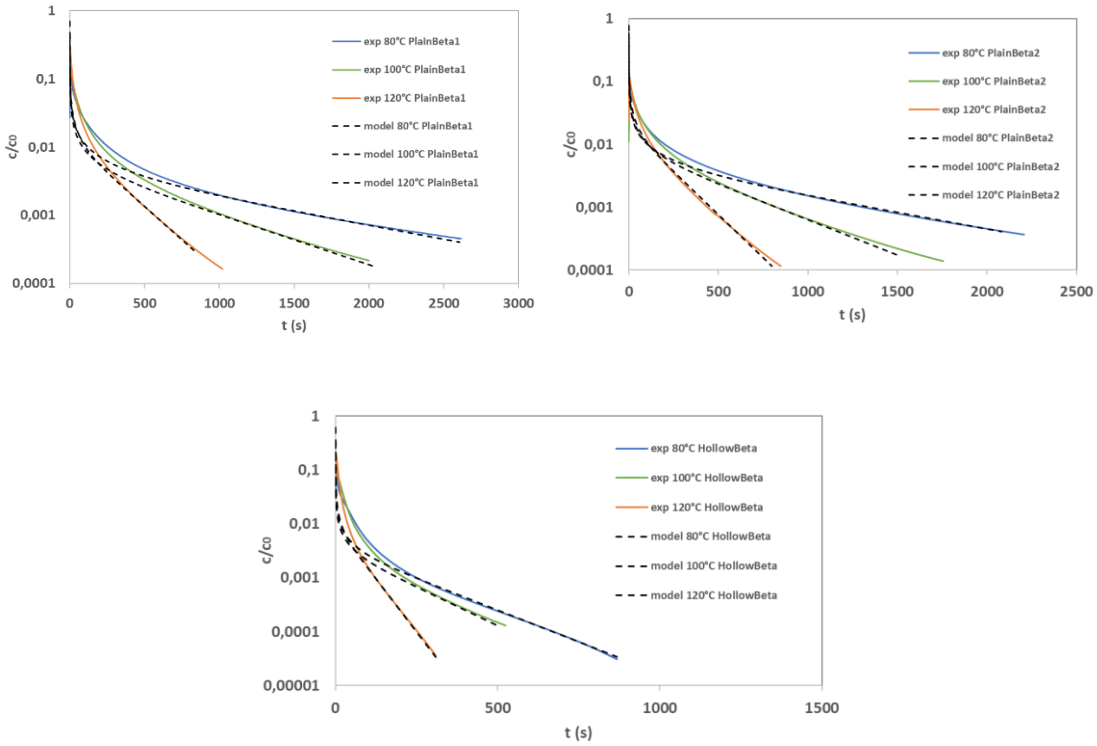


Figure 4 - Experimental ZLC data (plain lines) and theoretical ZLC curves (dashed lines) for cyclohexane desorption for Beta zeolites at 80, 100 & 120°C.

The effective diffusion energy E_d was obtained from the Arrhenius plot (see Figure E *1*). The effective energy of diffusion E_d found in Silicalite-1 samples, 27 kJ/mol, is consistent with the E_d found by similar studies in the literature (21-26 kJ/mol)[13], which underpins the validity of our results. Regarding cyclohexane transport in Beta zeolite, there are no available ZLC studies over Beta zeolite in the literature. Nevertheless, the E_d value found for cyclohexane transport through Beta samples (44.8-46.7 kJ/mol) is

comparable to the values found in the literature for cyclohexane through MFI-type zeolite by the ZLC technique (38-56 kJ/mol)[11,12,14,15,29].

The effective diffusion coefficients D_{eff} of plain zeolites were estimated from the characteristic time of diffusion (ZLC) and equivalent radius size estimated from microscopy images (Table *1*). The diffusion coefficients for **PlainS-1 (**R_{eq} = 70nm) is in the range of 1.5-3 x 10^{-18} m^2/s at 40-60°C. The study of the sorption kinetics of toluene in MFI zeolites by the ZLC technique has already been reported in the literature[13,30] for crystal sizes of ~2 µm. The authors found diffusion coefficients of 1.2 x 10^{-16} to 4.8 x 10^{-16} m^2/s, but at higher temperatures (80-120 °C) than in this study and with ZSM-5 crystals instead of Silicalite-1, which prevents the direct comparison of results. **PlainBeta1** (R_{eq} = 490 µm) and **PlainBeta2** (R_{eq}=330 µm) present D_{eff} coefficients in the range of 10^{-16}-10^{-17} m^2/s. Unfortunately, to the best of our knowledge, diffusion measurements of cyclohexane in Beta zeolites have not been reported. Nevertheless, we can observe that the values fall in the range of D_{eff} values found for **MFI** zeolites with relatively comparable crystal size, for the same temperature range, despite the difference of pore diamter between **MFI** and ***BEA**. For example, Teixeira *et al*.[14] present D_{eff} values of around 10^{-17} m^2/s between 70-110ºC, for Silicalite-1 crystals of R~0.34 µm, and Li *et al*.[11] present D_{eff} values of around 10^{-17} m^2/s between 70-90ºC, for ZSM-5 crystals of R~0.43 µm.

Table 2 - Characteristic diffusion times of toluene in Silicalite-1 zeolites.

Sample	T(°C)	**τ** (s)	**D_{eff} (m^2/s)**
PlainS-1	40	3236	1.51 x 10^{-18}
	50	2703	1.81 x 10^{-18}
	60	1712	2.86 x 10^{-18}
HollowS-1	40	1645	-
	50	1445	-
	60	1134	-

Table 3 - Characteristic diffusion times of cyclohexane in Beta zeolites.

Sample	T(°C)	τ (s)	D_{eff} (m^2/s)
PlainBeta1	80	10460	2.30×10^{-17}
	100	5848	4.11×10^{-17}
	120	2193	1.09×10^{-16}
PlainBeta2	80	8197	1.33×10^{-17}
	100	4167	2.61×10^{-17}
	120	1613	6.75×10^{-17}
HollowBeta	80	1822	-
	100	1495	-
	120	544	-

The same approach could have been carried out for the determination of effective diffusion coefficients for hollow zeolites, by taking the wall thickness as the equivalent radius. Instead, we have preferred to estimate the mean diffusion path of hollow zeolites, assuming that the effective diffusion was equal for hollow and plain zeolites. In the case of Silicalite-1 zeolites, the characterization carried out over the samples shows that **HollowS-1** and **PlainS-1** have similar physical and chemical properties in terms of crystal size, composition, external surface and N_2 physisorption. Consequently, we can assume that the diffusion coefficients D_{eff} of **HollowS-1** and **PlainS-1** are equal. For Beta samples, even though we observed differences between hollow and plain zeolites in terms either of external surface or slightly different Si/Al, we can assume that the diffusion coefficients of hollow and plain Beta zeolites are nearly equal. Hence, we can postulate that the square root of the ratio between the characteristic diffusion times of hollow and plain zeolites $(\tau_H/\tau_P)^{1/2}$ is equal to the ratio of their mean diffusion path lengths L_H/L_P (equation 1).

$$\sqrt{\frac{\tau_H}{\tau_P}} = \sqrt{\frac{\frac{L_H^2}{D_{eff}}}{\frac{L_P^2}{D_{eff}}}} = \frac{L_H}{L_P} \qquad \text{Eq.1}$$

We can now compare the ratio of diffusion path lengths (L_H/L_P) estimated by ZLC measurements and the ratio of equivalent radii (R_H/R_P) estimated from microscopy images of hollow and plain zeolites, considering a ± 10% error in the τ and R values (Table *4*).

For Silicalite-1 samples, we calculated a L_H/L_P ratio from ZLC measurements in the range of 0.64-0.90, depending on temperature. The R_H/R_P ratio obtained from microscopy images is between 0.58 to 0.71. We can conclude that the lengths estimated

by diffusion measurements and microscopy are in very good agreement, considering experimental errors and the assumptions made.

Table 4 - Comparison of diffusion path lengths of hollow and plain samples.

	T(ºC)	L_H/L_P ± 10 % error (ZLC data)	R_H/R_P ± 10 % error (microscopy images)
HollowS-1 vs. PlainS-1	40	0.64 – 0.75	0.58 – 0.71
	50	0.66 – 0.81	
	60	0.74 – 0.90	
HollowBeta vs. PlainBeta1	80	0.38 - 0.46	0.25 – 0.37
	100	0.46 - 0.56	
	120	0.45 - 0.55	
HollowBeta vs. PlainBeta2	80	0.43 – 0.52	0.37 – 0.56
	100	0.54 – 0.66	
	120	0.53 – 0.64	

The same approach was applied to compare hollow and plain morphologies of Beta crystals. In this case, **HollowBeta** is independently compared to **PlainBeta1** and then **PlainBeta2**. Similarly, to Silicalite-1 samples, the ratio of L_H/L_P obtained from characteristic diffusion time values is not very temperature-sensitive and it is in the range of 0.38-0.56 for **HollowBeta** and **PlainBeta1,** and 0.43-0.66 for **HollowBeta** and **PlainBeta2,** (Table 4). On the other hand, the equivalent radius ratios are between 0.25 to 0.37 and 0.37 to 0.56 upon comparison to **PlainBeta1** and **PlainBeta2,** respectively**.**

For the two zeolite-substrate systems, we can conclude that there is a good agreement between the ratio of the characteristic lengths estimated by ZLC and the ratio of the mean diffusion lengths measured from microscopy images. It should be noted that the $\mathbf{R_{eq}}$ might have a significant experimental error associated with the measurement itself, which may explain the differences observed between the two ratios. Indeed, measurements obtained by SEM and/or TEM images correspond on average to a relatively small population of 200-300 crystals. Moreover, in the case of **HollowS-1**, 20-30% of the crystals are not perfectly hollow structures, but rather multi-hollow structures for which $\mathbf{R_{eq}}$ values can hardly be estimated. The presence of a certain number of "broken" **HollowBeta** crystals might also induce some error in the R_H/R_P value.

The work of Novruzova *et al.*[31] is the only example in the literature that studies the impact of hollow zeolites on diffusion, but using a different sorbate and a different technique from that used in the present study. The authors studied the adsorption kinetics of isooctane in four different Silicalite-1 samples by comparing the uptake curves obtained by in situ diffuse reflectance FT-IR spectroscopy. Two of the samples were the plain and hollow Silicalite-1 zeolites used in this work and the two others consisted of large plain crystals (40 x 10 µm) and their corresponding multi-hollow analogs. The presence of holes in large

crystals induced faster isooctane uptake than in the corresponding bulk. On the other hand, the same uptake curve was observed on small crystals **HollowS-1** and **PlainS-1** zeolites, contrary to our results. The authors assumed that external surface barriers are the dominant mechanism in diffusion, which prevails on intracrystalline diffusion in smaller crystals. Although the conclusions may appear contradictory, it should be noted that the conditions and measurement techniques differ: i) the sorbates are different (isooctane instead of cyclohexane), ii) measurement temperatures are 150°C for Novruzova *et al*. vs. 40-60°C in this study, and iii) adsorption uptake measured in the crystal vs. desorption measured in the gas phase. We can assume that while the diffusion in silicalite-1 can be controlled by surface barrier aspects for isooctane whereas the diffusion of cyclohexane is not in the tested conditions. We want also to stress that surface barrier contribution cannot be ruled out in the case of cyclohexane. In the case it would occur, it would be a minor contribution to the overall resistance which cannot be quantified here taking into account of size dispersion of the crystals.

4. Conclusions

The experimental conditions were set to place the transport kinetics under a diffusion-controlled regime. In these conditions, we have demonstrated that hollow zeolites allow faster transport than plain zeolites due to the shortening of diffusion path length and importantly for same particle dimensions. For hollow Silicalite-1, the transport is doubled, while for hollow Beta zeolite it is quadrupled for crystals of very similar sizes and without a secondary porous network – attesting to the relevancy of this study.

Nomenclature

c – concentration of a given sorbent (mol/m^3)

c_0 – initial concentration of a given sorbate in the gas phase (mol/m^3)

D_{eff} – effective or apparent intracrystalline diffusion coefficient, of a whole crystal particle (m^2/s)

D_{eff}/L^2 – parameter extracted from the ZLC model, corresponding to the inverse of the characteristic transport time (s^{-1})

E_d – diffusion energy i.e. the energy required by a molecule to diffuse through the crystal (kJ/mol)

F – is the volumetric flow rate (m^3/s)

K_H – Henry's Law constant (dimensionless)

L – Mean diffusion path length or diffusion path length (m)

L_P – Mean diffusion path length or diffusion path length for plain zeolites (m)

L_H – Mean diffusion path length or diffusion path length for hollow zeolites (m)

L_{ZLC} – ZLC parameter

V_{cat} – zeolite volume (m^3)

Greek symbols

βn – ZLC parameter

τ — characteristic transport time or diffusion time through the crystals, obtained by ZLC model and defined as L^2/D_{eff} (s)

Appendix A - Characterization of Silicalite-1 samples

TEM images of PlainS-1 and HollowS-1 are presented in Figure A 1, and Figure A 2 respectively.

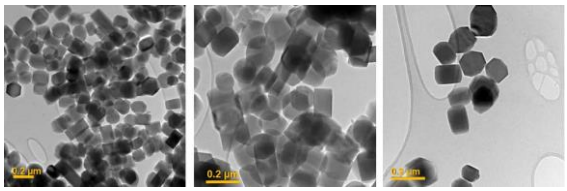


Figure A 1 - TEM images of **PlainS-1**.

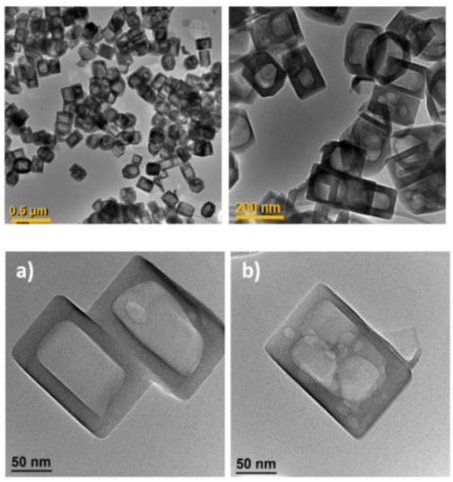


Figure A 2 - TEM images of **HollowSil1**.

Nitrogen adsorption/desorption isotherms of the considered samples are shown in Figure A 3. **PlainS-1** presents a type I adsorption branch at low pressure, which is typical of a microporous material. HollowS-1 also present a Type I adsorption branch, confirming the microporous nature of the zeolite walls and it presents a desorption branch with a hysteresis, which has been associated with condensation phenomena in the inner cavity. Adsorption data of the samples are summarized in **Error! Reference source not found.**, showing that both samples present very similar textural properties, with high microporous volume, high BET surface, and small mesoporous volume.

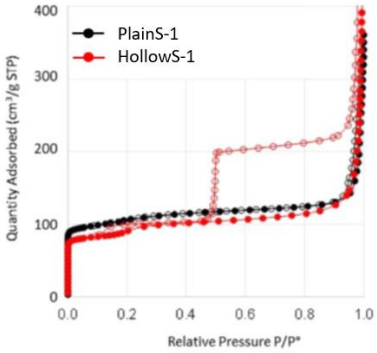


Figure A 3 - N_2 adsorption isotherms of PlainS-1 and HollowS-1, according to Laprune *et al*.[22]

Table A 1 - Textural properties of the samples PlainS-1 and HollowS-1, according to Laprune *et al*.[22]

Sample name	**PlainS-1**	**HollowS-1**
Isotherms type according to IUPAC	Type I	Type I + hysteresis
BET [m^2/g]	390	328
V_{micro} [cm^3/g]	0.13	0.12
V_{meso} [cm^3/g]	0.07	0.08

Appendix B - Characterization of Beta samples

XRD patterns of the Beta samples are presented in Figure B 1. TEM and SEM images of the three samples are shown in Figure B 2. We consider that PlainBeta1 has an ellipsoid, which dimensions R1 and R2 were measured from microscopy images, see Figure B 3.

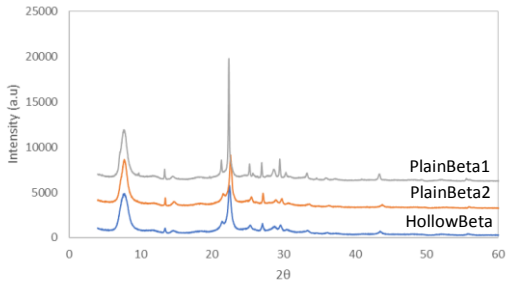


Figure B 1 - XRD patterns of **PlainBeta1, PlainBeta2** and **HollowBeta** samples.

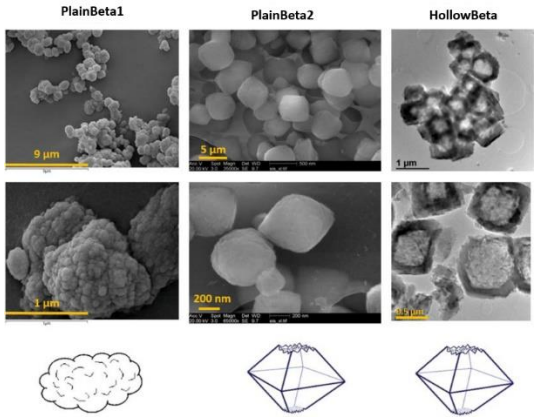


Figure B 2 - Electronic microscopic images of the three Beta samples, **PlainBeta1, PlainBeta2** and **HollowBeta**, and the respective external morphology representations bellow.

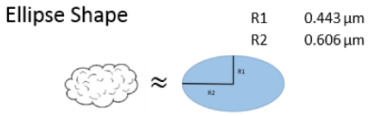


Figure B 3 - External morphology and dimensions for **PlainBeta1**.

Nitrogen adsorption/desorption isotherms of the considered samples are shown in Figure B 4. As already described in the paper, both bulk samples present a Type I adsorption branch, proving that the crystal is mainly microporous. **HollowBeta** also present a Type I adsorption branch, confirming the microporous nature of the zeolite walls, but it also presents a desorption branch with a hysteresis, which has been associated with condensation phenomena in bottle neck pores, as discussed in Morgado Prates *et al.*[18]. Some pore structure parameters are listed in Table B 1, the three samples present high V_{micro} and S_{BET}, even though **Plain1Beta** presents the smaller S_{BET}. V_{meso} are small and approximately the same for the three samples.

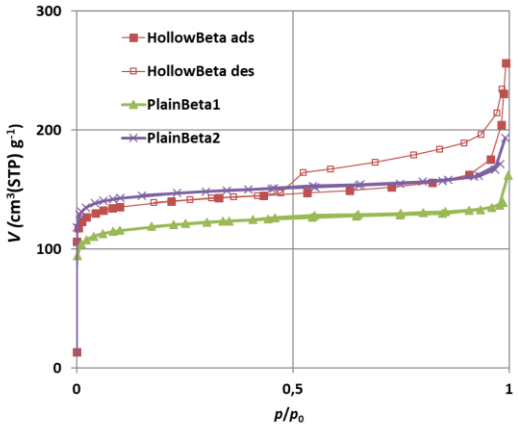


Figure B 4 - N_2 adsorption isotherms of **PlainBeta1** (triangles), **PlainBeta2** (crosses) and **HollowBeta** (squares).

Table B 1 - Textural properties of the samples **PlainBeta1**, **PlainBeta2** and **HollowBeta**.

Sample	Isotherm type	S_{BET} [m^2/g]	V_{micro} [cm^3/g]	V_{meso} [cm^3/g]
PlainBeta1	Type I	500	0.15	0.06
PlainBeta2	Type I	564	0.18	0.06
HollowBeta	Type I + hysteresis	542	0.16	0.09

Appendix C – ZLC Model

Data were analyzed considering the ZLC analysis of desorption curves developed by Eic and Ruthven[26]. The model considers a very thin layer of adsorbent uniformly equilibrated with a gas phase, and a certain adsorbate concentration c_0. It is assumed that external film mass transfer is fast enough to ensure that, under purging conditions, the sorbate concentration is very low not only in the bulk gas but also at the crystal surface. When neglecting hold-up in the gas phase, and assuming an adsorbent with a spherical shape of radius L, the transient mass balance for diffusion can be expressed in terms of effluent concentration c such as:

$$\frac{c(t)}{c_0} = 2L \sum_{n=1}^{\infty} \frac{exp(-\frac{\beta_n^2 D_{eff} t}{L^2})}{\beta_n^2 + L_{ZLC}(L_{ZLC} - 1)} \qquad \text{Eq. C1}$$

Where β_n and L_{ZLC} are some parameters defined as:

$$\beta_n \, cot\beta_n \, + L_{ZLC} - 1 = 0 \qquad \text{Eq. C2}$$

$$L_{ZLC} = \frac{FL^2}{3V_{cat}K_H D_{eff}} \qquad \text{Eq. C3}$$

L_{ZLC} represents the ratio of purge flow rate and the diffusional time constant, where F is the volumetric flow rate, L is the radius of the spherical particle, V_{cat} is the adsorbent volume, K_H is the Henry's constant if adsorption takes place within Henry's region and D_{eff} is the effective diffusion coefficient. The L_{ZLC} value expressed how far the system is for equilibrium.[32]

When the purge **flow rate (F) is high**, the system is in the kinetically controlled regime, L_{ZLC} is large and $\beta = n\pi$; so the equation is simplified to:

$$\frac{c(t)}{c_0} = 2L \sum_{n=1}^{\infty} \frac{exp(-\frac{n^2\pi^2 D_{eff} t}{L^2})}{(n\pi)^2 + L_{ZLC}(L_{ZLC} - 1)} \qquad \text{Eq. C4}$$

On the long time region of the desorption curve, only the first term of the summation (n=1) is significant, and the summation becomes an asymptode:

$$ln\left(\frac{c(t)}{c_0}\right) = ln\left[\frac{2L_{ZLC}}{\beta_1^2 + L_{ZLC}(L_{ZLC} - 1)}\right] - \frac{\beta_1^2 \boldsymbol{D_{eff}}}{\boldsymbol{L^2}} \qquad \text{Eq. C5}$$

Under those conditions, we can determine the characteristic diffusion time $\boldsymbol{\tau = L^2 / D_{eff}}$ directly from the slopes of the asymptode.

In order to obtain reliable diffusivity data, we must ensure that the run is made under kinetic transport regime. In our study, we have used the value of the parameter L_{ZLC} as an indicator of the regime, where L_{ZLC} should be greater than 10 for assuring kinetic regime[14].

Appendix D – ZLC Set-up

Figure D 1 shows a simplified schematic diagram of the ZLC set-up. The **adsorption line** (in green) carries a low concentration of sorbate diluted in He. This is prepared by dilution of a low flow saturated stream with a relatively large flow He bypass. The low flow saturated stream was prepared by passing a small He flow through a bubbler, maintained at low temperature by a Julabo ED (V.2) low temperature thermostat. The **desorption line** (in blue) is a high flow He line. Both adsorption and desorption streams are feed by a mass flow controller, MF1, MF2 and MF3. The "Switch valve" controls which of the two streams (adsorption or desorption) are delivered to the ZLC cell, that is placed in a gas chromatograph oven (Agilent, 6850 Series GC system). Two pressure indicators are placed before the switching valve, one on the adsorption line – PI Ads – and the other on the desorption line – PI Des. These continuously control the pressure of each stream, and pressure drops during each run. The effluent stream from the ZLC cell is continuously monitored by a flame ionization detector (FID). The effluent concentration response is recorded after the valve switch to desorption.

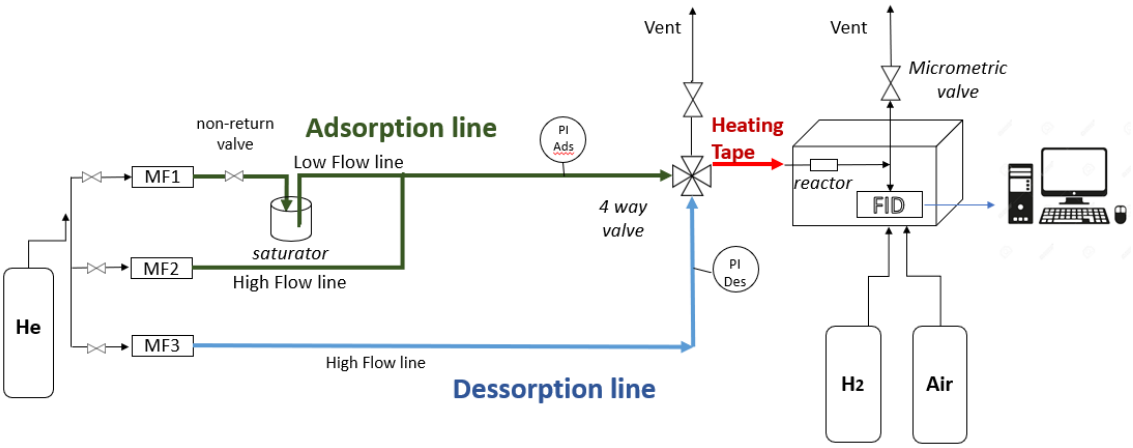


Figure D 1 - Zero Length Column (ZLC) experimental set-up.

Appendix E – ZLC Results

Table E 1 present the diffusion parameters extracted from the theoretical fitting of the ZLC over the desorption curves. All L_{ZLC} values are greater than 10, showing that the processes are in the diffusion controlled regime[14].

Table E 1 - Parameters τ and L_{ZLC}, extracted from ZLC desorption curves.

Sample	T(°C)	L_{ZLC}	τ (s)
PlainS-1	40	24	3236
	50	17	2703
	60	14	1712
HollowS-1	40	19	1645
	50	16	1445
	60	14	1134
PlainBeta1	80	427	10460
	100	365	5848
	120	158	2193
PlainBeta2	80	401	8197

	100	239	4167
	120	113	1613
	80	533	1822
HollowBeta	100	570	1495
	120	218	544

The Arrhenius plots for toluene and Silicalite-1 sample and cyclohexane and Beta samples are presented in Figure E 1.

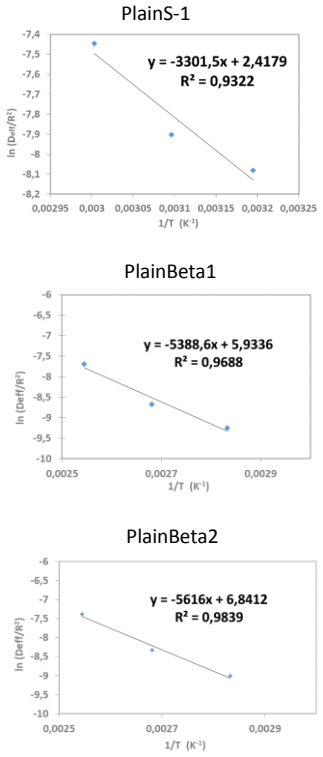


Figure E 1- Arrhenius plots for toluene and **PlainS-1** and for cyclohexane and Plain Beta samples.

References

[1] J. Pérez-Ramírez, C.H. Christensen, K. Egeblad, C.H. Christensen, J.C. Groen, Hierarchical zeolites: enhanced utilisation of microporous crystals in catalysis by advances in materials design, Chem. Soc. Rev. 37 (2008) 2530–2542. https://doi.org/10.1039/B809030K.

[2] D. Verboekend, J. Pérez-Ramírez, Design of hierarchical zeolite catalysts by desilication, Catal. Sci. Technol. 1 (2011) 879–890. https://doi.org/10.1039/C1CY00150G.

[3] M. Hartmann, A.G. Machoke, W. Schwieger, Catalytic test reactions for the evaluation of hierarchical zeolites, Chem. Soc. Rev. 45 (2016) 3313–3330. https://doi.org/10.1039/C5CS00935A.

[4] D.P. Serrano, J.M. Escola, P. Pizarro, Synthesis strategies in the search for hierarchical zeolites, Chem. Soc. Rev. 42 (2013) 4004–4035. https://doi.org/10.1039/C2CS35330J.
[5] C.J. Van Oers, W.J.J. Stevens, E. Bruijn, M. Mertens, O.I. Lebedev, G. Van Tendeloo, V. Meynen, P. Cool, Formation of a combined micro- and mesoporous material using zeolite Beta nanoparticles, Microporous Mesoporous Mater. 120 (2009) 29–34. https://doi.org/10.1016/j.micromeso.2008.08.056.
[6] S.C. Larsen, Nanocrystalline Zeolites and Zeolite Structures: Synthesis, Characterization, and Applications, J. Phys. Chem. C. 111 (2007) 18464–18474. https://doi.org/10.1021/jp074980m.
[7] L. Tosheva, V.P. Valtchev, Nanozeolites: Synthesis, Crystallization Mechanism, and Applications, Chem. Mater. 17 (2005) 2494–2513. https://doi.org/10.1021/cm047908z.
[8] S. Mintova, M. Jaber, V. Valtchev, Nanosized microporous crystals: emerging applications, Chem. Soc. Rev. 44 (2015) 7207–7233. https://doi.org/10.1039/C5CS00210A.
[9] M. Choi, K. Na, J. Kim, Y. Sakamoto, O. Terasaki, R. Ryoo, Stable single-unit-cell nanosheets of zeolite MFI as active and long-lived catalysts, Nature. 461 (2009) 246–9. https://doi.org/10.1038/nature08288.
[10] D. Schneider, D. Mehlhorn, P. Zeigermann, J. Kärger, R. Valiullin, Transport properties of hierarchical micro–mesoporous materials, Chem. Soc. Rev. 45 (2016) 3439–3467. https://doi.org/10.1039/C5CS00715A.
[11] C. Li, Y. Ren, J. Gou, B. Liu, H. Xi, Facile synthesis of mesostructured ZSM-5 zeolite with enhanced mass transport and catalytic performances, Appl. Surf. Sci. 392 (2017) 785–794. https://doi.org/10.1016/j.apsusc.2016.09.054.
[12] C.-C. Chang, A.R. Teixeira, C. Li, P.J. Dauenhauer, W. Fan, Enhanced Molecular Transport in Hierarchical Silicalite-1, Langmuir. 29 (2013) 13943–13950. https://doi.org/10.1021/la403706r.
[13] H. Zhao, J. Ma, Q. Zhang, Z. Liu, R. Li, Adsorption and Diffusion of n-Heptane and Toluene over Mesoporous ZSM-5 Zeolites, Ind. Eng. Chem. Res. 53 (2014) 13810–13819. https://doi.org/10.1021/ie502496v.
[14] A. Teixeira, C.-C. Chang, T. Coogan, R. Kendall, W. Fan, P. Dauenhauer, Dominance of Surface Barriers in Molecular Transport through Silicalite-1, J. Phys. Chem. C. 117 (2013) 25545–25555. https://doi.org/10.1021/jp4089595.
[15] W.L. Duncan, K.P. Möller, On the Diffusion of Cyclohexane in ZSM-5 Measured by Zero-Length-Column Chromatography, Ind. Eng. Chem. Res. 39 (2000) 2105–2113. https://doi.org/10.1021/ie9907573.
[16] L. Gueudré, E. Jolimaître, N. Bats, W. Dong, Diffusion in zeolites: is surface resistance a critical parameter?, Adsorption. 16 (2010) 17–27. https://doi.org/10.1007/s10450-010-9213-6.
[17] J. Pérez-Ramírez, D. Verboekend, A. Bonilla, S. Abelló, Zeolite Catalysts with Tunable Hierarchy Factor by Pore-Growth Moderators, Adv. Funct. Mater. 19 (2009) 3972–3979. https://doi.org/10.1002/adfm.200901394.
[18] A.R. Morgado Prates, C. Pagis, F.C. Meunier, L. Burel, T. Epicier, L. Roiban, S. Koneti, N. Bats, D. Farrusseng, A. Tuel, Hollow Beta Zeolite Single Crystals for the Design of Selective Catalysts, Cryst. Growth Des. 18 (2018) 592–596. https://doi.org/10.1021/acs.cgd.7b01635.
[19] C. Pagis, A.R. Morgado Prates, D. Farrusseng, N. Bats, A. Tuel, Hollow Zeolite Structures: An Overview of Synthesis Methods, Chem. Mater. 28 (2016) 5205–5223. https://doi.org/10.1021/acs.chemmater.6b02172.
[20] C. Pagis, F. Meunier, Y. Schuurman, A. Tuel, M. Dodin, R. Martinez-Franco, D. Farrusseng, Demonstration of Improved Effectiveness Factor of Catalysts Based on Hollow Single Crystal Zeolites, ChemCatChem. 10 (2018). https://doi.org/10.1002/cctc.201801225.
[21] C. Pagis, C. Bouchy, M. Dodin, R.M. Franco, D. Farrusseng, A. Tuel, Hollow Y zeolite single crystals: synthesis, characterization and activity in the hydroisomerization of n-hexadecane, Oil Gas Sci. Technol. – Rev. D'IFP Energ. Nouv. 74 (2019) 38. https://doi.org/10.2516/ogst/2019015.
[22] D. Laprune, A. Tuel, D. Farrusseng, F.C. Meunier, Highly Dispersed Nickel Particles Encapsulated in Multi-hollow Silicalite-1 Single Crystal Nanoboxes: Effects of Siliceous Deposits and Phosphorous Species on the Catalytic Performances, ChemCatChem. 9 (2017) 2297–2307. https://doi.org/10.1002/cctc.201700233.
[23] S. Li, T. Boucheron, A. Tuel, D. Farrusseng, F. Meunier, Size-selective hydrogenation at the subnanometer scale over platinum nanoparticles encapsulated in silicalite-1 single crystal hollow shells, Chem. Commun. Camb. Engl. 50 (2014). https://doi.org/10.1039/c3cc48648f.
[24] J. Zheng, Q. Zeng, Y. Zhang, Y. Wang, J. Ma, X. Zhang, W. Sun, R. Li, Hierarchical Porous Zeolite Composite with a Core−Shell Structure Fabricated Using β-Zeolite Crystals as Nutrients as Well as Cores, Chem. Mater. 22 (2010) 6065–6074. https://doi.org/10.1021/cm101418z.
[25] L. Ding, Y. Zheng, Z. Zhang, Z. Ring, J. Chen, Effect of agitation on the synthesis of zeolite beta and its synthesis mechanism in absence of alkali cations, Microporous Mesoporous Mater. 94 (2006) 1–8. https://doi.org/10.1016/j.micromeso.2006.03.010.
[26] M. Eic, D.M. Ruthven, A new experimental technique for measurement of intracrystalline diffusivity, Zeolites. 8 (1988) 40–45. https://doi.org/10.1016/S0144-2449(88)80028-9.
[27] M.A. Camblor, A. Corma, S. Valencia, Characterization of nanocrystalline zeolite Beta, Microporous Mesoporous Mater. 25 (1998) 59–74. https://doi.org/10.1016/S1387-1811(98)00172-3.
[28] Y. Kamimura, W. Chaikittisilp, K. Itabashi, A. Shimojima, T. Okubo, Critical Factors in the Seed-Assisted Synthesis of Zeolite Beta and "Green Beta" from OSDA-Free Na+–Aluminosilicate Gels, Chem. – Asian J. 5 (2010) 2182–2191. https://doi.org/10.1002/asia.201000234.
[29] F.D. Magalhães, R.L. Laurence, Wm.C. Conner, Diffusion of Cyclohexane and Alkylcyclohexanes in Silicalite, J. Phys. Chem. B. 102 (1998) 2317–2324. https://doi.org/10.1021/jp972036s.
[30] D. Xu, J. Ma, H. Zhao, Z. Liu, R. Li, Adsorption and diffusion of n-heptane and toluene over mesostructured ZSM-5 zeolitic materials with acidic sites, Fluid Phase Equilibria. 423 (2016) 8–16. https://doi.org/10.1016/j.fluid.2016.04.013.
[31] N. Novruzova, A. Tuel, D. Farrusseng, F.C. Meunier, Influence of crystal size on the uptake rate of isooctane in plain and hollow silicalite-1 crystals, Microporous Mesoporous Mater. 228 (2016) 147–152. https://doi.org/10.1016/j.micromeso.2016.03.039.
[32] E. Mangano, S. Brandani, D.M. Ruthven, Analysis and Interpretation of Zero Length Column Response Curves, Chem. Ing. Tech. 85 (2013) 1714–1718. https://doi.org/10.1002/cite.201300083.

Credit Author Statement

A.R. Morgado : Investigation*, Formal Analysis, Writing -original draft, Visualization, Validation ;* ***C. Daniel****: Methodology, Data Curation ;* ***C. Pagis****: Investigation;* ***Y. Schuurman:*** *Supervision;* **A. Tuel:** *Project administration, Writing – Review & Editing;* **D.Farrusseng:** *Conceptualization, Writing – Review & Editing, Funding acquisition*

Declaration of Interest:
The authors declare no competing financial interest.